Asian Journal of Chemistry; Vol. 37, No. 9 (2025), 2237-2243
ASIAN JOURNAL OF CHEMISTRY
https://doi.org/10.14233/ajchem.2025.34334

One-Step Formation of CoV_2O_6 Nanostructure and its Photocatalytic Activity

R. JAYANTHI[1], R. SURESH[1,2,*] and N. JAYAPRAKASH[3]

[1]Department of Chemistry, Karpagam Academy of Higher Education, Coimbatore-641021, India
[2]Centre for Material Chemistry, Karpagam Academy of Higher Education, Coimbatore-641021, India
[3]Department of Chemistry, SRM Valliammai Engineering College (Autonomous), Kattankulathur-603203, India

*Corresponding author: E-mail: sureshinorg@gmail.com

Received: 25 June 2025 *Accepted*: 12 August 2025 *Published online*: 30 August 2025 AJC-22104

A one-step thermal decomposition method was proposed for the synthesis of cobalt vanadate (CoV_2O_6) nanostructures using ammonium metavanadate (NH_4VO_3) and cobalt acetate [$Co(CH_3COO)_2{\cdot}4H_2O$] as precursors. No solvents and additional chemicals were used in this synthesis method. The as-prepared CoV_2O_6 nanostructure was characterized by energy dispersive X-ray spectroscopy (EDS), X-ray diffraction (XRD), Fourier-transform infrared (FTIR) and Raman spectroscopic techniques. These techniques determined the crystallinity, crystal structure and metal-oxygen (V-O and Co-O) bonds of CoV_2O_6 nanostructure. Ultraviolet (UV)-visible spectroscopic study infers the characteristic electronic transitions and band-gap energy of CoV_2O_6 nanostructure. The electron microscopic investigations affirmed the formation of nanostructured particles. All studies concluded the formation of CoV_2O_6 nanostructure. The photocatalytic ability of CoV_2O_6 nanostructure in the degradation (decolourization) of methylene blue, sunset yellow and brilliant blue dyes in presence of visible light and hydrogen peroxide was evaluated. The CoV_2O_6 nanostructure showed a maximum efficiency towards a methylene blue degradation reaction.

Keywords: Cobalt vanadate, Photocatalyst, Methylene blue, Sunset yellow, Brilliant blue, Degradation.

INTRODUCTION

Metal vanadates are a class of compounds composed of vanadium (V), oxygen (O) and other metals. Metal vanadates are widely studied for their application in supercapacitors, batteries, hydrogen generation, nitrogen fixation and carbon dioxide reduction [1,2]. Metal vanadates have also been studied for their catalytic application in the field of water pollution mitigation. For instance copper vanadate ($Cu_3V_2O_8$) nanorods were used as a photocatalyst to degrade different organic dyes under 500 W xenon lamp illumination and the maximum efficiency (73%) of $Cu_3V_2O_8$ nanorods is reported for brilliant blue degradation [3]. Zinc vanadate ($Zn_3V_2O_8$) nanoparticles with photocatalytic activity in the degradation of crystal violet dye under ultraviolet (UV) illumination have been reported [4]. Silver vanadate ($AgVO_3$) nanorods with 85.02% of methylene blue degradation efficiency (visible light condition) is also reported [5]. In another study, a complete degradation of rhodamine B under UV light irradiation was demonstrated by using bismuth vanadate (α-$Bi_4V_2O_{11}$) photocatalyst [6]. In the metal vanadate series, cobalt vanadates could also be employed as catalysts due to their moderate band-gap energy and effective charge separation tendency [7]. Cobalt vanadates can be prepared by various methods such as solid-state synthesis [8], co-precipitation [9], combustion [10], hydrothermal [7] and sol-gel approach [11]. There are different forms (*i.e.* different molecular formula) of cobalt vanadates including CoV_2O_6 [11], $Co_2V_2O_7$ [7] and $Co_3V_2O_8$ [7] and their formation is mainly dependent precursors and synthesis method [7,12,13]. Hence, the selection of synthesis methods is crucial to obtain a particular form of cobalt vanadate. In this background, this study focused to synthesis a cobalt vanadate nanostructure by a one-step thermal decomposition method without using any reagents including a solvent and surfactant.

Water pollutants containing synthetic dyes have serious environmental concerns because of their mutagenic and carcinogenic properties [14]. Dye pollutants cause harmful effects to human, aquatic animals and plants [15]. As a result of toxicities, it is important to remove these organic dyes from wastewater and it can be achieved by different treatments including

This is an open access journal, and articles are distributed under the terms of the Attribution 4.0 International (CC BY 4.0) License. This license lets others distribute, remix, tweak, and build upon your work, even commercially, as long as they credit the author for the original creation. You must give appropriate credit, provide a link to the license, and indicate if changes were made.

sonocatalysis, adsorption, photocatalysis and catalytic reduction processes [16,17]. Among the dye treatment techniques, photocatalytic processes have advantages including high removal efficiency, dye mineralization efficiency and possibility to utilize solar light [18-20]. However, some pristine metal vanadates show poor photocatalytic activity due to their rapid recombination of photogenerated charge carriers [21]. But, addition of an oxidizing reagent such as H_2O_2 could improve the photocatalytic performance of the photocatalytic materials [22]. In this context, the synthesized cobalt vanadate nanostructure was tested as a photocatalyst in the degradation of methylene blue, sunset yellow and brilliant blue dyes in presence of H_2O_2 and visible light conditions.

In this work, the synthesis of CoV_2O_6 nanostructure by one-step thermal decomposition method was described and the prepared sample was characterized by different spectroscopic and electron microscopic techniques. The photocatalytic activity of CoV_2O_6 nanostructure was explored by using visible light-assisted oxidative degradation of methylene blue, sunset yellow and brilliant blue dyes.

EXPERIMENTAL

Ammonium metavanadate (NH_4VO_3), cobalt acetate tetrahydrate ($(CH_3COO)_2Co{\cdot}4H_2O$), methylene blue, brilliant blue and sunset yellow dyes were purchased from Sisco Research Laboratories (India), whereas 30% w/v H_2O_2 was purchased from Isochem Laboratories (India). Double distilled water was used as a solvent for photocatalytic experiments.

Synthesis procedure: A one-step thermal decomposetion method was adopted to prepare CoV_2O_6 nanostructure. In a procedure, 0.0075 mol (0.877 g) of NH_4VO_3 and 0.0025 mol (0.623 g) of $(CH_3COO)_2Co{\cdot}4H_2O$ were mixed homogeneously in a mole ratio in a mortar with pestle for about 30 min manually and the aforementioned mixture was subsequently taken in a silica crucible, kept in a muffle furnace and calcined for 4 h at 500 ºC. After cooling to room temperature, the resulting powder was collected, finely ground and used for characterization and photocatalytic studies

Instrumentation: The synthesized powder was investigated by using a Bruker D8 enhanced diffractometer (Germany) with Cu$K\alpha_1$ radiation (λ = 1.5406 Å). SHIMADZU 8300 Fourier transform infrared spectrometer (Japan) was used to record a FTIR spectrum in the range of 4000-400 cm^{-1}. The Raman spectrum of the synthesized powder was recorded by using a HORIBA LabRam HR Evolution microscope with the laser wavelength = 532 nm, precision = 0.4 cm^{-1}. JASCO V-750 UV-visible spectrophotometer (Japan) was employed to obtain a DRS UV-visible spectrum of the powder. Barium sulphate ($BaSO_4$) was used as a reference. Thermo Scientific Apreo S high-resolution scanning electron microscope with FEI QUANTA 200 energy dispersive spectroscopy (Germany) and JEM-2100 high-resolution transmission electron microscope were used to capture SEM and TEM images, respectively.

Photocatalytic studies: To explore the photocatalytic activity of the synthesized CoV_2O_6 nanostructure, a H_2O_2-assisted photocatalytic degradation of methylene blue, sunset yellow and brilliant blue dyes under visible light irradiation was employed. The photocatalytic experiments were carried out in a HEBER photocatalytic reactor (India) which consists of a 160 W xenon lamp as a visible light source. The photocatalytic reaction aliquot was prepared by dispersing (sonication for 10 min) 30 mg of CoV_2O_6 nanostructure powder in 1×10^{-5} M (100 mL) dye solution. The reaction aliquot was stirred by using a magnetic stirrer for 30 min (without light) to achieve an adsorption/desorption equilibrium. After that the photocatalytic reaction mixture was taken into a borosilicate glass tube, added 100 µL of H_2O_2 and then started the visible light illumination. The dye samples were collected for every 15 min time interval, centrifuged and the supernatant liquid was analyzed through a UV-visible spectrophotometer (a reference solvent was double distilled water) with the wavelength range of 800-340 nm. The methylene blue, sunset yellow and brilliant blue degradation reactions were monitored by noting absorption maximum at 664, 483 and 628 nm, respectively. The photocatalytic degradation efficiency (E %) was estimated using the following relation:

$$E = \frac{A_o - A_t}{A_o} \times 100$$

where A_o and A_t are initial and final absorbance of maximum peak.

RESULTS AND DISCUSSION

Formation of CoV_2O_6 nanostructure: The salts, NH_4VO_3 and $(CH_3COO)_2Co{\cdot}4H_2O$ were physically mixed and the resultant solid mixture was heated at 500 ºC. The recorded EDS spectrum of the synthesized powder (Fig. 1) shows several energy peaks with variable intensities. A peak appearing at ~0.5 keV is due to oxygen (O), while characteristic vanadium (V)-related peaks occur at ~4.9 and ~5.4 keV [11]. High intense peaks at ~0.7, ~6.9 and ~7.6 keV correspond to (Co) cobalt [11]. The occurrence of these peaks confirm that the final product is composed of Co, V and O elements only. The absence of peaks due to nitrogen (N) and carbon (C) indicates that the salts undergo thermal decomposition with elimination of nitrogen and carbon as ammonia and CO_2/methane gaseous products. Studies found that thermal decomposition of NH_4VO_3 leads to form V_2O_5 and NH_3 gas [23], while the thermal decomposition of $(CH_3COO)_2Co{\cdot}4H_2O$ forms cobalt oxide, water vapour, acetone, carbon dioxide, *etc.* [24].

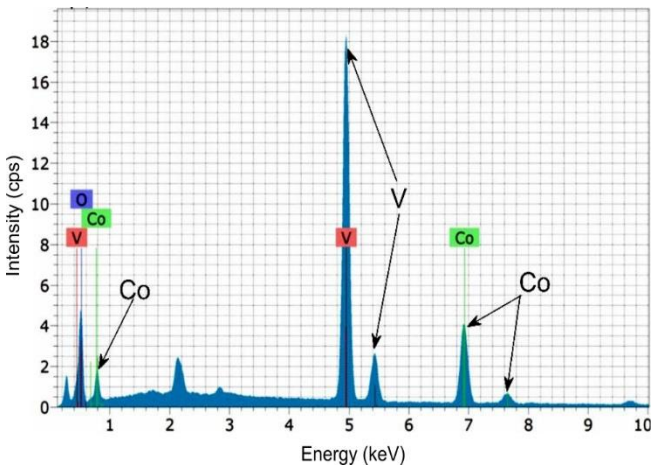

Fig. 1. EDS spectrum of CoV_2O_6 nanostructure

The XRD analysis is helpful to predict the structure of a crystalline material. Hence, the synthesized powder, composed of Co, V and O was analyzed by XRD technique and the obtained result is shown as Fig. 2. The XRD pattern shows that the counts of a maximum intense peak are about 150 counts. The diffraction peaks are observed at 20.3º, 27.4º, 28.7º, 29.3º, 32.9º, 38.9º and 52.1º, which correspond to (-201), (110), (201), (111), (-311), (-402) and (-204) crystal planes of monoclinic structured CoV_2O_6 (ICDD No: 01-077-1174). On the other hand, the weak intense peaks present at 26.2º and 31.0º are due to (110) and (031) crystal planes of orthorhombic structured V_2O_5 (ICDD No: 01-085-0601) [25]. These results reveal that thermal decomposition of $NH_4VO_3/(CH_3COO)_2Co{\cdot}4H_2O$ mixture takes place at 500 ºC and forms CoV_2O_6 nanostructure along with V_2O_5 impurity. It should be mentioned that CoV_2O_6 nanoparticles have been prepared by a hydrothermal [26] and co-precipitation [27] methods. But the present method did not use any solvent and additional reagent to obtain a CoV_2O_6 nanostructure. The crystallite size (D) of the CoV_2O_6 nanostructure has been calculated from the Scherrer's equation [28] and the obtained value is found to be 67 nm.

$$D = \frac{K\lambda}{\beta \cos\theta}$$

(where K = 0.98, λ = X ray wavelength, θ = diffraction angle and β = full width at half of the maximum)

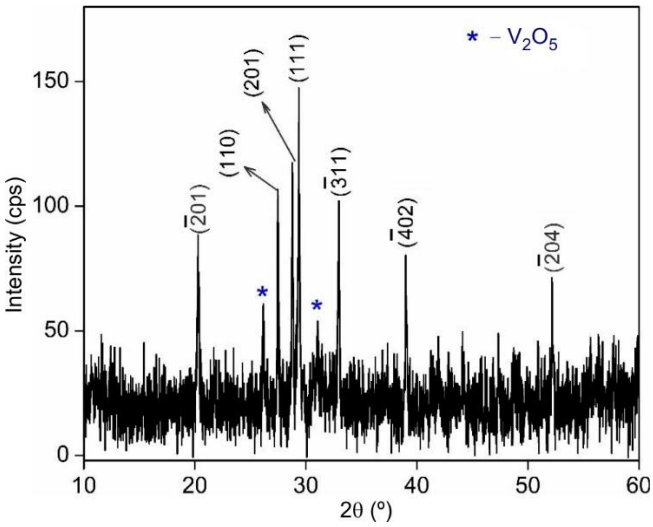

Fig. 2. XRD pattern of CoV_2O_6 nanostructure

The FTIR analysis is useful to find the metal-oxygen groups of a metal oxide nanomaterials [29]. Fig. 3 shows four distinct peaks at 512, 626, 811 and 1018 cm^{-1} in the range of 1100 to 500 cm^{-1}. The peaks present at 1018 cm^{-1} can be assigned to terminal stretching vibration of $V\text{-}O_1$ (terminal), whereas a band occurring at 811 cm^{-1} is related to $V\text{-}O_2\text{-}V$ (bridging) stretching vibrations [30]. The peaks appeared at 626 and 512 cm^{-1} are due to $3V\text{-}O_3$ stretching and $V\text{-}O_2\text{-}V$ deformation, respectively [30]. According to Yasodha *et al.* [31], the Co-O stretching vibrations appear at 602 and 522 cm^{-1}. These peaks may be overlapped with $V\text{-}O_3/V\text{-}O_2$ stretching/deformation peaks. The broad and weak bands present at 3415 and 1631 cm^{-1} are due to O-H stretching and bending vibrations of water molecules [32].

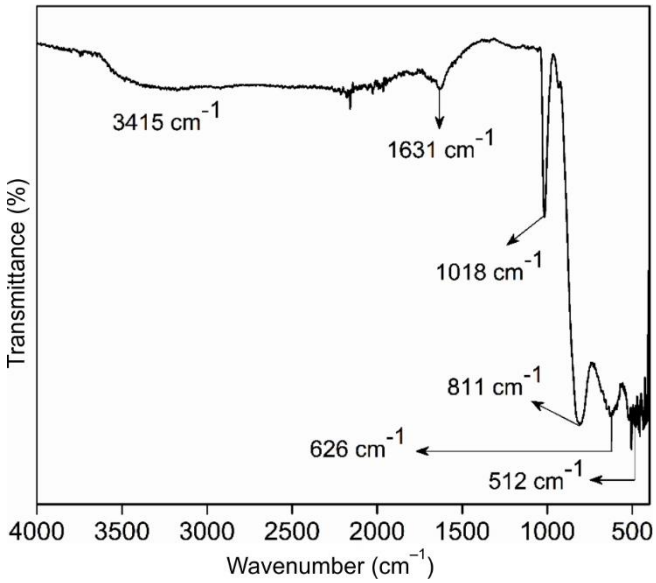

Fig. 3. FT-IR spectrum of CoV_2O_6 nanostructure

The Raman spectrum (Fig. 4) shows the characteristic vibrational modes of CoV_2O_6 [33,34]. There are Raman bands at 104, 130, 180, 318, 464, 669 and 804 cm^{-1}. A predominant Raman band at 804 cm^{-1} ($B_{2g}{}^{12}$) is correlated to V-O stretching vibration, whereas a band present at 318 cm^{-1} ($A_g{}^6$) is caused from $V\text{-}O_2$ bending mode. The lattice related vibration can be observed at 130 cm^{-1} ($B_{3g}{}^2$). Other bands at 104, 180, 464 and 669 cm^{-1} are due to $A_{2g}{}^1$, $B_{3g}{}^3$, $A_g{}^{10}$ and $A_g{}^{12}$ modes, respectively [34]. Both FTIR and Raman results further supported the XRD result of the CoV_2O_6 nanostructure.

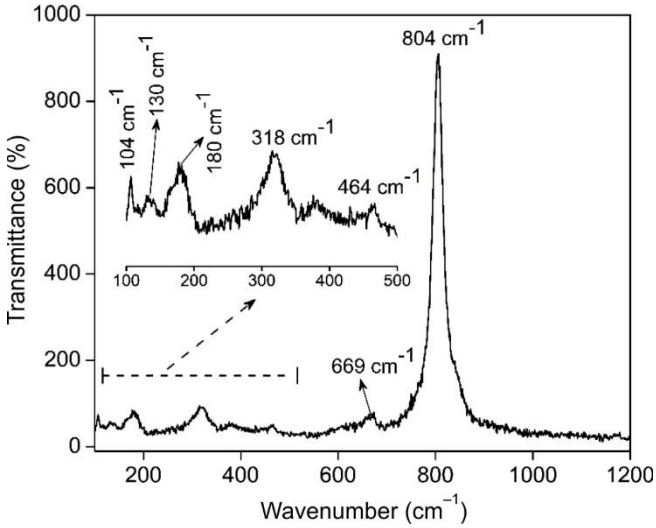

Fig. 4. Raman spectrum of CoV_2O_6 nanostructure

The UV-visible absorption spectrum was recorded for CoV_2O_6 nanostructure (Fig. 5). In the visible region, three absorption peaks were observed at 464, 609 and 709 nm. The absorption peak present at 464 nm is attributed to the charge transfer transitions from the O 2p to V 3d [35], whereas the Co^{2+} *d-d* transition can be observed at 609 nm [36]. An absorption peak that appears at 709 nm might be related to vanadium with variable oxidation states [37]. The Tauc's plot was drawn using an equation, $(\alpha h\nu)^2 = A(h\nu - E_g)$ (absorption coefficient,

Planck constant, frequency and absorbance are denoted by α, h, ν and A, respectively) to find the band gap energy of CoV_2O_6 nanostructure (inset in Fig. 5). The computed band gap energy of the CoV_2O_6 nanostructure is 1.6 eV, which is consistent with other report [38].

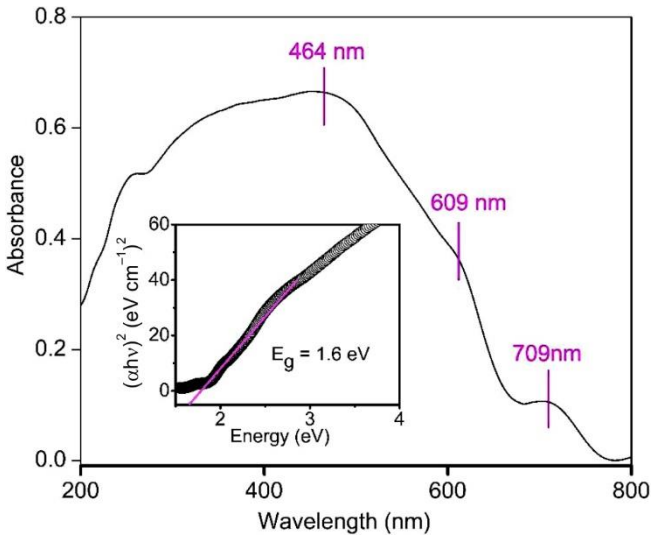

Fig. 5. DRS UV-visible absorption spectrum of the CoV_2O_6 nanostructure. Inset shows the Tauc's plot of CoV_2O_6 nanostructure

Morphology: The morphology and surface features of CoV_2O_6 powder was determined by SEM and HR-TEM results. A SEM image (Fig. 6a) clearly shows the arrangement of oval shaped particles with variable sizes. The boundaries of each particle can also be seen clearly and the average particle size is about 458 nm. In addition, rod and sphere-like particles are co-existed with the oval shaped particles (Fig. 6b). Individual oval shaped particles were formed by combining fine particles. Significantly, large pores/gaps are visible on the surface of particles. The presence of pores in the nanomaterials is beneficial for its catalytic activity [39]. HRTEM images of fine particles at different magnifications are shown in Fig. 7a-c. The fine particles have different shapes such as rectangle, circle and ellipse. The crystalline feature of CoV_2O_6 powder was further validated by selected area diffraction pattern (Fig. 7d), as observed by the bright spots in the image [40].

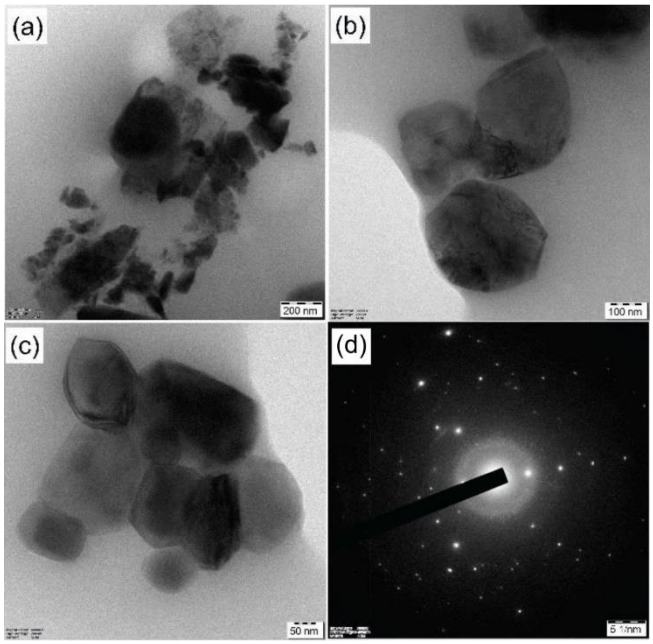

Fig. 7. HRTEM images (a-c) and (d) SAED pattern of CoV_2O_6 nanostructure

Photocatalytic activity: The H_2O_2-assisted photocatalytic activity of the synthesized CoV_2O_6 nanostructure has been assessed under visible light irradiation and the obtained results are discussed as follows:

Degradation of methylene blue: Methylene blue is a stable (cationic) thiazine dye which is not readily degraded under visible light irradiation or H_2O_2 alone. Consequently, a photocatalyst is desirable for the fast degradation of methylene blue dye in water. Hence, the synthesized CoV_2O_6 nanostructure was tested as a photocatalyst and the obtained results are shown as Fig. 8. The absorption spectrum of pure methylene blue dye shows a prominent peak at 665 nm, due to the thiazine unit of methylene blue monomer [41]. Also, a shoulder peak at 613 nm that corresponds to dimer of methylene blue mole-

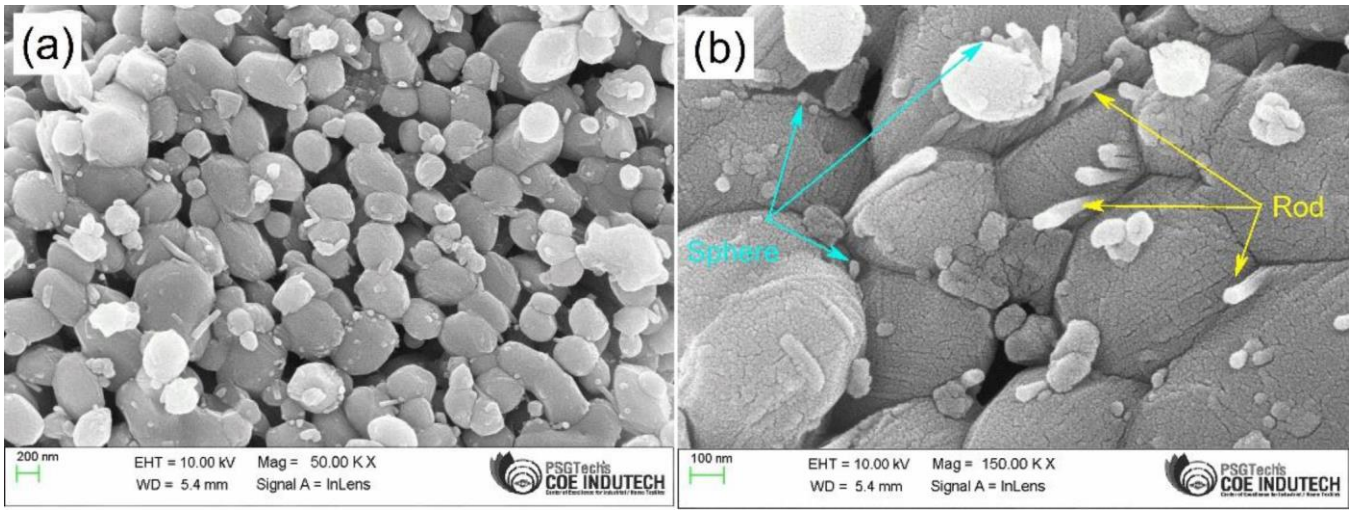

Fig. 6. HRSEM images (a, b) of CoV_2O_6 nanostructure

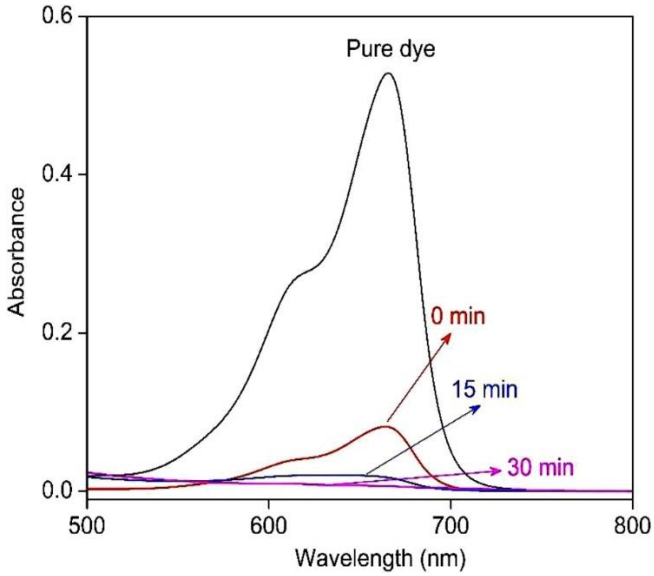

Fig. 8. Absorbance spectra of methylene blue dye in presence of visible light/H_2O_2/CoV_2O_6

cules [41]. After the dark experiment (*i.e.* adsorption-desorption equilibrium), a remarkable decline of absorbance at 665 nm can be observed, which might be due to the effective adsorption of methylene blue molecules on the surface of CoV_2O_6 nanostructure. In spite of a change in a shoulder peak, no remarkable shift in a maximum peak position was observed. Illumination of visible light in addition with H_2O_2 leads to further decline in absorbance of a peak maxima. This result indicates that when methylene blue dye was exposed to visible light/H_2O_2/CoV_2O_6, the chromophore was diminished. About 92.8% of methylene blue degradation efficiency was observed after 30 min of the photocatalytic reaction. The obtained photocatalytic efficiency of CoV_2O_6 for methylene degradation is comparable to Sr-doped $BiVO_4$ nanoparticles [42], CeO_2/graphene oxide/polyacrylamide [43] and nitrogen doped carbon quantum dots/zeolitic imidazolate framework (ZIF)-8 [44] photocatalysts.

Degradation of sunset yellow: Sunset yellow is an anionic azo dye, which is not readily degraded under visible light illumination. Herein, CoV_2O_6/H_2O_2/visible light system was used to degrade the sunset yellow dye in water medium. The obtained photocatalytic results are shown as Fig. 9. An aqueous solution of a pure sunset yellow dye shows a maximum absorption peak at 483 nm, which corresponds to the orange-red colour of sunset yellow molecules [45]. The adsorption-desorption experiment (0 min) leads to a 35.4% decrease in absorbance at 483 nm, indicating an interaction occurs between the sunset yellow and CoV_2O_6 nanostructure. After starting the visible light illumination and the addition of H_2O_2, a remarkable decrease in absorbance (from 0.42 to 0.19) at 483 nm is observed within 30 min and the corresponding photocatalytic efficiency is 54.8%. In addition, a slight shift towards a lower wavelength (from 483 to 477 nm) is also observed. It infers the breaking of azo bonds by the CoV_2O_6/H_2O_2/visible light system. A further continuation of a visible light irradiation leads to a small decrease of absorbance and the final efficiency was obtained as 72% after 135 min.

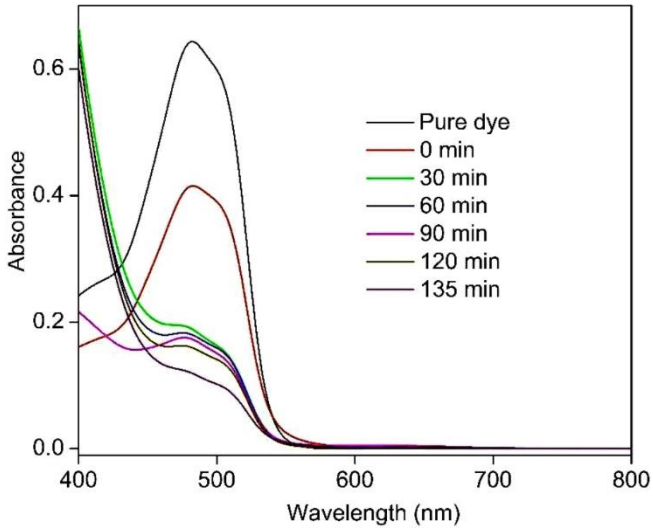

Fig. 9. Absorbance spectra of sunset yellow dyes in presence of visible light/H_2O_2/CoV_2O_6

Degradation of brilliant blue: Brilliant blue is a triarylmethane (anionic) dye which shows toxicity [46]. Studies on the degradation of brilliant blue in water have been reported [47,48]. The synthesized CoV_2O_6 has also been applied as a photocatalyst to degrade brilliant blue (Fig. 10). The absorption spectrum of a pure brilliant blue dye solution displays a peak at 693 nm, corresponding to the blue colour [47]. At 0 min, the absorbance was decreased from 0.97 to 0.80 and the corresponding adsorption efficiency is 17.5%. In presence of H_2O_2 and visible light illumination for 150 min, the absorbance maxima is decreased from 0.80 to 0.70 (photocatalytic efficiency = 12.5%). These results suggest that the degradation of brilliant blue is not favourable in presence of CoV_2O_6.

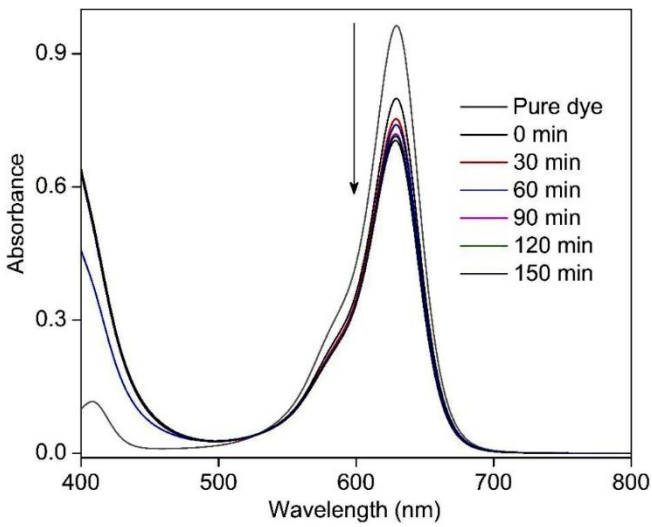

Fig. 10. Absorbance spectra of brillian blue dye in presence of visible light/H_2O_2/CoV_2O_6

Photocatalytic mechanism: The above results conclude that CoV_2O_6 nanostructure is found to be the best photocatalyst for the degradation of methylene blue dye when compared to sunset yellow dye and brilliant blue dyes. In order to find the methylene blue degradation mechanism, further photocatalytic reactions were performed with additional charge

trapping reagents. In this study, KI and $K_2S_2O_8$ were used as a hole and electron scavenging reagent, respectively [49]. Separate photocatalytic experiments with 1 mmol of KI and $K_2S_2O_8$ was performed for 30 min and the obtained result is shown in Fig. 11. The degradation efficiency of methylene blue decreased from 92.8% in the absence of a scavenging agent to 84.2% upon hole scavenging, and further to 68.4% in the presence of an electron scavenger. This result indicates that the photogenerated electrons have a major role in CoV_2O_6 nanostructure-assisted photocatalytic degradation of methylene blue when compared to photogenerated holes. Based on the experimental results, the efficient degradation of methylene blue on the surface of CoV_2O_6 nanostructures can be described as follows: under visible light illumination, electrons in the valence band of CoV_2O_6 are excited to the conduction band, generating holes in the valence band. The excited electrons will react with H_2O_2 to form hydroxyl ($^{\bullet}OH$) radicals, which could effectively degrade the methylene blue molecules [50].

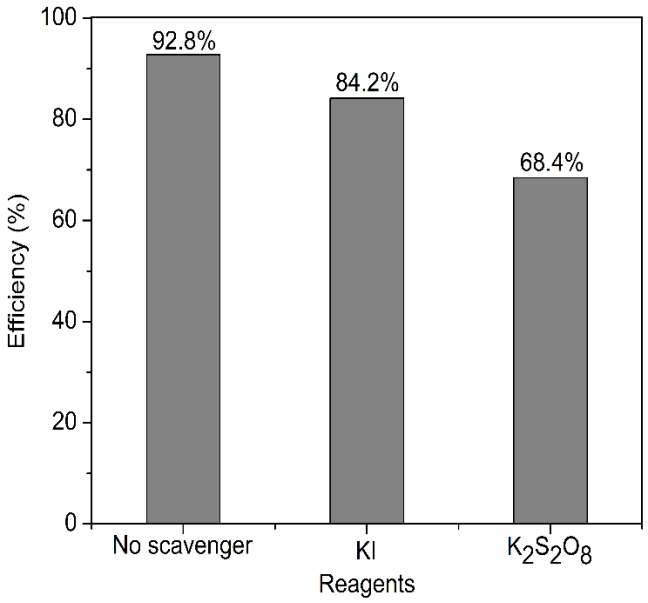

Fig. 11. Photocatalytic efficiency of CoV_2O_6 in presence of KI and $K_2S_2O_8$ scavenging agent. Light source = visible light; Oxidant = H_2O_2

Conclusion

A CoV_2O_6 nanostructure was successfully synthesized *via* a one-step thermal decomposition method without the use of any solvents or additional chemicals. The formation of CoV_2O_6 nanostructures was confirmed by X-ray diffraction (XRD), Fourier-transform infrared (FT-IR) and Raman spectroscopic analyses. CoV_2O_6 nanostructure absorbs visible light effectively and its band gap is 1.6 eV. The CoV_2O_6 nanostructure particles have different morphologies. CoV_2O_6 nanostructure showed about 92.8% (30 min) photocatalytic efficiency towards methylene blue, whereas it shows 72% (135 min) and 12.5% (150 min) efficiency in the photocatalytic degradation of sunset yellow and brilliant blue, respectively. The present synthesis method might also be used to synthesize other metal vanadates. CoV_2O_6 nanostructure will become a good photocatalyst in the treatment of dye-based wastewater.

ACKNOWLEDGEMENTS

The authors acknowledge Central Instrumentation Facility (SCIF) and Nanotechnology Research Centre (NRC), SRMIST, Tamil Nadu, India for the provision of characterization facilities.

CONFLICT OF INTEREST

The authors declare that there is no conflict of interests regarding the publication of this article.

REFERENCES

1. J. Banerjee and K. Dutta, *Int. J. Energy Res.*, **46**, 3983 (2022); https://doi.org/10.1002/er.7492
2. I. Ahmad, G. Li, A. Al-Qattan, A.J. Obaidullah, A. Mahal, M. Duan, K. Ali, Y.Y. Ghadi and I. Ali, *Mater. Today Sustain.*, **25**, 100666 (2024); https://doi.org/10.1016/j.mtsust.2024.100666
3. A. George, S. Rahul, A. Dhayal Raj, Q. Yang, G. Jayakumar, S. John Sundaram, M. Selvaraj, M.W. Alam, P. Rosaiah and J.V. Kumar, *Inorg. Chem. Commun.*, **168**, 112890 (2024); https://doi.org/10.1016/j.inoche.2024.112890
4. F. Tagnaouti Moumnani, K. Khallouk, R. Elkhalfaouy, D. Moussaid, O. Mertah, A. Solhy, A. Barakat and A. Kherbeche, *React. Kinet. Mech. Catal.*, **137**, 1157 (2024); https://doi.org/10.1007/s11144-023-02553-2
5. V. Sivakumar, R. Suresh, K. Giribabu and V. Narayanan, *Solid State Sci.*, **39**, 34 (2015); https://doi.org/10.1016/j.solidstatesciences.2014.10.016
6. S. Kumar and P.D. Sahare, *Nano*, **8**, 1350007 (2013); https://doi.org/10.1142/S1793292013500070
7. R. Lakshmana Naik, T. Bala Narsaiah, P. Justin, A. Naveen Kumar, M.N. Somashekar, N. Raghavendra, C.R. Ravikumar, A. Ahmad Khan and M.S. Santosh, *Mater. Sci. Eng. B*, **298**, 116861 (2023); https://doi.org/10.1016/j.mseb.2023.116861
8. M.T.H. Bhuiyan, M.A. Rahman, M.A. Rahman, R. Sultana, M.R. Mostafa, A.H. Tania and M.A.R. Sarker, *Cogent Physics*, **3**, 1265778 (2016); https://doi.org/10.1080/23311940.2016.1265778
9. E. Baudrin, S. Laruelle, S. Denis, M. Touboul and J.M. Tarascon, *Solid State Ion.*, **123**, 139 (1999); https://doi.org/10.1016/S0167-2738(99)00096-X
10. Y.T. Kim, K.B. Gopukumar, K.B. Kim and B.W. Cho, *J. Power Sources*, **112**, 504 (2002); https://doi.org/10.1016/S0378-7753(02)00462-7
11. D. von Dreifus, R. Pereira, A.D. Rodrigues, E.C. Pereira and A.J.A. de Oliveira, *Ceram. Int.*, **44**, 19397 (2018); https://doi.org/10.1016/j.ceramint.2018.07.171
12. M. Markkula, A.M. Arevalo-Lopez and J. Paul Attfield, *J. Solid State Chem.*, **192**, 390 (2012); https://doi.org/10.1016/j.jssc.2012.04.029
13. C.B. Liu, Z.Z. He, S.L. Wang, M. Yang, Y. Liu, Y.J. Liu, R. Chen, H.P. Zhu, C. Dong, J.Z. Ke, Z.W. Ouyang, Z.C. Xia and J.F. Wang, *J. Phys. Condens. Matter*, **31**, 375802 (2019); https://doi.org/10.1088/1361-648X/ab26fe
14. R.O. Alves de Lima, A.P. Bazo, D.M.F. Salvadori, C.M. Rech, D. de Palma Oliveira and G. de Aragão Umbuzeiro, *Mutat. Res. Genet. Toxicol. Environ. Mutagen.*, **626**, 53 (2007); https://doi.org/10.1016/j.mrgentox.2006.08.002
15. S. Kobylewski and M.F. Jacobson, *Int. J. Occup. Environ. Health*, **18**, 220 (2012); https://doi.org/10.1179/1077352512Z.00000000034
16. G. Wang and H. Cheng, *Molecules*, **28**, 3706 (2023); https://doi.org/10.3390/molecules28093706
17. Y. Wu, C. Wang, L. Wang and C. Hou, *Catalysts*, **15**, 391 (2025); https://doi.org/10.3390/catal15040391
18. M. Settu, G. Govindhan, B. Thirugnanam, D. Divya, M. Selvamani and M.R. Karim, *J. Inorg. Organomet. Polym. Mater.*, **35**, 2502 (2025); https://doi.org/10.1007/s10904-024-03381-0

19. S.O. Rab, F.M.A. Altalbawy, L. Baldaniya, A. Kumar, R. M M, M. Kundlas, G.C. Sharma, K.K. Joshi, S. Saydaxmetova and M.K. Abosaoda, *Inorg. Chem. Commun.*, **174**, 114067 (2025); https://doi.org/10.1016/j.inoche.2025.114067
20. P. Sasikala, J. Madhavan, T. Bavani, M. Preeyanghaa and B. Neppolian, *Chem. Phys.*, **592**, 112618 (2025); https://doi.org/10.1016/j.chemphys.2025.112618
21. M. El ouardi, M. Arab, M. Saadi, A. BaQais and H. Ait Ahsaine, *Nano Mater. Sci.*, (2024); https://doi.org/10.1016/j.nanoms.2024.11.002
22. M.A. Ali, I.M. Maafa and I.Y. Qudsieh, *Water*, **16**, 453 (2024); https://doi.org/10.3390/w16030453
23. T. Zhang and Q. Li, *J. Solid State Chem.*, **315**, 123473 (2022); https://doi.org/10.1016/j.jssc.2022.123473
24. T. Wanjun and C. Donghua, *Chem. Pap.*, **61**, 329 (2007); https://doi.org/10.2478/s11696-007-0042-3
25. D. Govindarajan, V. Uma Shankar and R. Gopalakrishnan, *J. Mater. Sci. Mater. Electron.*, **30**, 16142 (2019); https://doi.org/10.1007/s10854-019-01984-9
26. M.A. Yewale, A.V.S.L. Sai Bharadwaj, R.A. Kadam, N.T. Shelke, A.M. Teli, S.A. Beknalkar, V. Kumar, M.W. Alam and D.K. Shin, *Mater. Sci. Eng. B*, **307**, 117464 (2024); https://doi.org/10.1016/j.mseb.2024.117464
27. X. He, J. Jiang, H. Tian, Y. Niu, Z. Li, Y. Hu, J. Fan and C. Wang, *RSC Adv.*, **9**, 9475 (2019); https://doi.org/10.1039/C8RA10041A
28. S.A. Hassanzadeh-Tabrizi, *J. Alloys Compd.*, **968**, 171914 (2023); https://doi.org/10.1016/j.jallcom.2023.171914
29. S. Pasieczna-Patkowska, M. Cichy and J. Flieger, *Molecules*, **30**, 684 (2025); https://doi.org/10.3390/molecules30030684
30. A. Surca and B. Orel, *Electrochim. Acta*, **44**, 3051 (1999); https://doi.org/10.1016/S0013-4686(99)00019-5
31. P. Yasodha, M. Premila, A. Bharathi, M.C. Valsakumar, R. Rajaraman and C.S. Sundar, *J. Solid State Chem.*, **183**, 2602 (2010); https://doi.org/10.1016/j.jssc.2010.09.003
32. N. Kotov, M.M. Keskitalo and C.M. Johnson, *Spectrochim. Acta A Mol. Biomol. Spectrosc.*, **330**, 125640 (2025); https://doi.org/10.1016/j.saa.2024.125640
33. J.P. Peña, P. Bouvier, M. Hneda, C. Goujon and O. Isnard, *J. Phys. Chem. Solids*, **154**, 110034 (2021); https://doi.org/10.1016/j.jpcs.2021.110034
34. J. Sánchez-Martín, P. Bouvier, G. Garbarino, S. Gallego-Parra, O. Isnard, P. Rodríguez-Hernández, A. Muñoz, D. Errandonea and J. Pellicer-Porres, *J. Phys. Chem. C*, **129**, 10364 (2025); https://doi.org/10.1021/acs.jpcc.5c02341
35. S.K. Jayaraj, V. Sadishkumar, T. Arun and P. Thangadurai, *Mater. Sci. Semicond. Process.*, **85**, 122 (2018); https://doi.org/10.1016/j.mssp.2018.06.006
36. E. Gungor, T. Gungor, D. Caliskan and E. Ozbay, *Acta Phys. Pol. A*, **131**, 500 (2017); https://doi.org/10.12693/APhysPolA.131.500
37. K. Schneider, *J. Mater. Sci. Mater. Electron.*, **31**, 10478 (2020); https://doi.org/10.1007/s10854-020-03596-0
38. S. Zang, X. Cai, M. Chen, D. Teng, F. Jing, Z. Leng, Y. Zhou and F. Lin, *Nanomaterials*, **12**, 1931 (2022); https://doi.org/10.3390/nano12111931
39. S. Estrada-Flores, A. Martínez-Luévanos, C.M. Perez-Berumen, L.A. García-Cerda and T.E. Flores-Guia, *Bol. Soc. Esp. Ceram. Vidr.*, **59**, 209 (2020); https://doi.org/10.1016/j.bsecv.2019.10.003
40. Y. Zhou, Y. Wu, D. Guo, J. Li, D. Chu, S. Na, M. Yu, D. Li, G. Sui and D.F. Chai, *J. Alloys Compd.*, **963**, 171133 (2023); https://doi.org/10.1016/j.jallcom.2023.171133
41. S. Mondal, M.E. De Anda Reyes and U. Pal, *RSC Adv.*, **7**, 8633 (2017); https://doi.org/10.1039/C6RA28640B
42. P.K. Panda, R. Kamal, R. Pattanaik, D. Pradhan and S.K. Dash, *Asian J. Chem.*, **37**, 123 (2024); https://doi.org/10.14233/ajchem.2025.32904
43. Z. Kalaycıoğlu, B. Özuğur Uysal, Ö. Pekcan and F.B. Erim, *ACS Omega*, **8**, 13004 (2023); https://doi.org/10.1021/acsomega.3c00198
44. A.A. Abd El Khalk, M.A. Betiha, A.S. Mansour, M.G. Abd El Wahed and A.M. Al-Sabagh, *ACS Omega*, **6**, 26210 (2021); https://doi.org/10.1021/acsomega.1c03195
45. A.T. Bişgin, *J. AOAC Int.*, **101**, 1850 (2018); https://doi.org/10.5740/jaoacint.18-0089
46. A. Soni, D.C. Parameswarappa, M. Tyagi, N.K. Sahoo, A. Dogra, R.R. Pappuru and J. Chhablani, *Semin. Ophthalmol.*, **37**, 117 (2022); https://doi.org/10.1080/08820538.2021.1928717
47. D. Negoescu, P. Oancea, A. Răducan and M. Puiu, *Rev. Roum. Chim.*, **66**, 281 (2021); https://doi.org/10.33224/rrch.2021.66.3.08
48. M. Alamzeb, S. Faryad, I. Ullah, J. Hussain and W.N. Setzer, *J. Fluoresc.*, (2025); https://doi.org/10.1007/s10895-025-04218-w
49. M. Pannerselvam, V. Siva, A. Murugan, A.S. Shameem, T. Bavani, S. Jhelai, S. Shanmugan, I.H.S. Ali and K. Kannan, *Nanomaterials*, **15**, 545 (2025); https://doi.org/10.3390/nano15070545
50. Y. Cao, Y. Ren, J. Zhang, T. Xie and Y. Lin, *Opt. Mater.*, **121**, 111637 (2021); https://doi.org/10.1016/j.optmat.2021.111637